Ab initio molecular-dynamics study of the structural, vibrational, and electronic properties of glassy GeSe$_2$

Mark Cobb, D. A. Drabold, and R. L. Cappelletti

Department of Physics and Astronomy, Condensed Matter and Surface Sciences Program, Ohio University, Athens, Ohio 45701-2979
(Received 20 May 1996)

We present results of an *ab initio* molecular-dynamics study of glassy GeSe$_2$ using a 216 atom model. The network topology of our model is analyzed through partial pair correlations, angle distributions, partial static structure factors, and ring structures. The total static structure factor and first sharp diffraction peak are in good agreement with experiment. The vibrational density of states and dynamical structure factor are in good agreement with experimental results as well. We have visualized the normal modes vectors in order to qualitatively understand their motion. The electronic density of states compares very well with experimental ultraviolet photoemission spectroscopy and x-ray photoemission spectroscopy measurements. The localization of the electronic states is analyzed. [S0163-1829(96)09141-2]

I. INTRODUCTION

The structural, vibrational, and electronic properties of binary alloy chalcogenide glasses are long standing areas of interest in the field of amorphous materials. Glassy germanium diselenide (g-GeSe$_2$) is one of the most intensely studied chalcogenide alloys. This glass is of particular interest for a number of reasons: its intermediate-range order, difficult interpretation of its vibrational dynamics, and very unusual electronic and optical properties which include photodarkening. Amorphous Ge-Se semiconductors have potential applications in optical storage devices, solar cells, and other such devices that require materials which are photosensitive.[1] In this paper we present a detailed theoretical study of the structural, vibrational, and electronic properties of the g-GeSe$_2$ using a 216 atom model.

This work has importance as an early *ab initio* study of a binary glass. It is not *a priori* obvious that the traditional molecular-dynamics method of simulating a liquid, cooling and quenching should lead to a credible model of a system exhibiting the complex ordering features of a glassy binary chalcogenide. We note that g-GeSe$_2$ is a particular challenge since the energy penalty for wrong bonds (Ge-Ge or Se-Se) is not so overwhelming as in SiO$_2$, which has also recently been studied with *ab initio* methods.[2] The primary concern is that the time scales accessible to the most efficient *ab initio* schemes are *far* too short compared to experiment, and this might be expected to have serious impact on a system exhibiting complex ordering. We demonstrate in this work that such systems are *surprisingly well* modeled with *ab initio* methods, even reproducing features like the first sharp diffraction peak, and the vibrational spectrum accurately. The structural and dynamical credibility of the models we propose implies that a broad range of theoretical work on stability, light-induced effects, and transport is accessible for these interesting materials.

In order to correctly model the chemistry and dynamics of g-GeSe$_2$ an *ab initio* approach must be employed. Determining the bonding configurations that Ge and Se will choose beyond the obvious Ge(Se$_{1/2}$)$_4$ tetrahedral configurations is not a simple matter. In a material such as SiO$_2$ the highly ionic nature of Si-O bonds makes wrong bonds less likely to occur,[2] but this is not the case for g-GeSe$_2$. The dynamics of g-GeSe$_2$ can only be properly characterized by a force scheme which includes the many-body effects derived from covalent bonding.

Our previous study of g-GeSe$_2$ focused on 62 and 63 atom models.[3] We found that our results for the structural and vibrational properties were in good agreement with experiment. Unfortunately these models were not large enough to adequately describe the intermediate-range order (IRO) of g-GeSe$_2$. In particular, the first peak of the static structure factor $S(Q)$ (a definite sign that IRO was present) was not well defined, suggesting that a larger model was required. The first sharp diffraction peak (FSDP) of $S(Q)$ in g-GeSe$_2$ indicates structural order on the range of approximately 6 Å but the precise structural characteristics responsible for it have yet to be determined. We find that there is a strong correlation between the FSDP and the fraction of edge-sharing Ge atoms. Our structural analysis focuses on the network topology and the chemical disorder of our model. Because we possess the *atomic coordinates* of a credible model, we can infer the microscopic origins of the experimentally measured structural features.

A significant difference between the vibrational density of states (VDOS) of our earlier studies and the experimental VDOS occurred around 20 meV. Our 62/63 atom models had significantly less spectral weight then the experimental VDOS in this region. The improvement between our model and experimental results we attribute to the Ge homopolar bonded structures which were not present in our smaller models. Our analysis of the model's dynamical properties focuses on regions of the vibrational density of states which have been studied extensively through Raman and inelastic neutron scattering and clearly elucidates the connection between experimental vibrational spectra and microscopic network modes of the material. Theory and experiment are compared directly through the VDOS and the dynamical structure factor $S(Q,E)$. We present an analysis of the normal mode dynamics based on species-projected density of

states, localization, and visual inspection using computer animation. This analysis of the dynamics, which would be impossible to obtain through experiment (in particular the visual analysis), provides us with a much deeper understanding of g-GeSe$_2$'s dynamics then was ever previously possible.

The electronic structure of our model is compared to experimental results through the electronic density of states and the localization of the electronic states is determined and compared to the results of previous theoretical studies. A question of fundamental importance is whether there are states in the gap between the valence and conduction bands.[1,4] One might expect that there would be a number of gap states due to topological defects but experimentally very few are actually observed. We find no gap states in any of our models despite the fact that they have large numbers of defects (onefold Se, threefold Se, threefold Ge).

II. MODEL

Computations described in this section used the *ab initio*, local basis density functional method of Sankey and co-workers.[5] The essential approximations are (1) Bachelet-Hamann-Schlüter pseudopotentials,[6] (2) the Harris functional,[7] (3) the local-density approximation,[8] and (4) a minimal basis set of one s and three p confined pseudo-atomic orbitals per site. The method has met with great success in a wide variety of systems, and provides a transferable description of covalently bonded materials. In addition, application of a self-consistent variant of this Hamiltonian produces similar results.[9]

A cubic supercell 18.76 Å on a side with 144 selenium atoms and 72 germanium atoms placed on a diamond lattice was chosen for the initial configuration of our model. This gave our model the correct stoichiometry and by construction a number density close to the experimental one of 3.339×10^{22} cm^{-3} (see Ref. 10). The initial temperature of the cell was 6000 K, it was then equilibrated to 5000 K over approximately 600 fs. The cell was then cooled to 1000 K and equilibrated at this temperature for approximately 1 ps. As a final step the system was slowly cooled to 300 K over 4 ps and then quenched to $T=0$ K. All of our calculations were done at constant volume using only the Γ point to sample the Brillouin zone. The Γ point is a suitable choice because of the small size of the Brillouin zone.

III. STRUCTURAL PROPERTIES

The topology of our model is determined through the partial pair-distribution functions (PDF's), angle distributions, and ring statistics. The static structure factor $S(Q)$ is calculated in order to have a direct comparison with experiment. The partial static structure factors are used to determine the contribution from the various real-space correlations (Ge-Ge,Ge-Se,Se-Se).

A. Static structure factor

In this work the static structure factor (Fig. 1) is computed as

$$S(Q) = 1 + \frac{1}{N\langle \overline{b}^2 \rangle} \sum_i \sum_{j,j \neq i} \overline{b}_i \overline{b}_j \frac{\sin(Q r_{ij})}{Q r_{ij}} . \qquad (1)$$
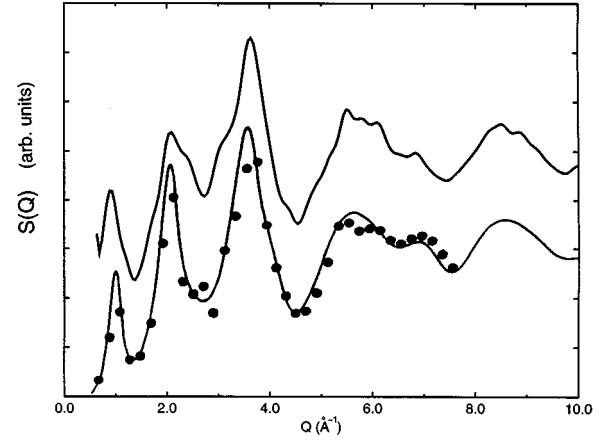

FIG. 1. The upper curve is the $S(Q)$ from our 216 atom model and the lower curve is $S(Q)$ data from Fig. 5 of Ref. 23.

The summations are over the atoms of the supercell, r_{ij} being the distance between atom i and atom j. The scattering length values taken from Ref. 10 are $b_{Ge}=0.819$ and $b_{Se}=0.797$ in units of 10^{-4} Å. The partial static structure factors (Fig. 2) are defined as

$$S_{\alpha\beta}(Q) = \frac{1}{N\langle \overline{b}^2 \rangle} \left(\sum_i^\alpha \sum_j^\beta \overline{b}_i \overline{b}_j \delta_{i,j} + \sum_i^\alpha \sum_{j,j \neq i}^\beta \overline{b}_i \overline{b}_j \frac{\sin(Q r_{ij})}{Q r_{ij}} \right) \qquad (2)$$

$$\langle \overline{b}^2 \rangle = \frac{N_\alpha \overline{b}_\alpha^2 + N_\beta \overline{b}_\beta^2}{N} , \qquad (3)$$
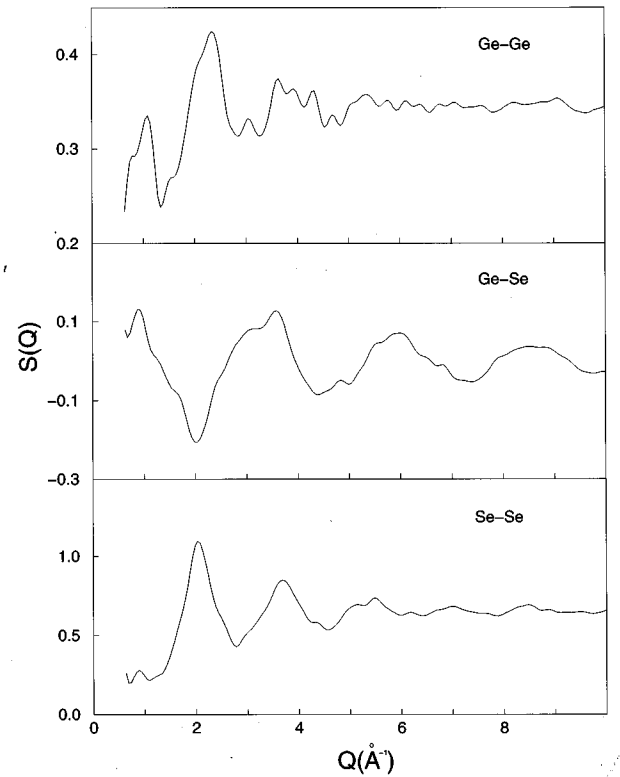

FIG. 2. Partial structure factors $S_{\alpha\beta}(Q)$ for 216 atom model.

$$S(Q) = S_{\text{Se-Se}}(Q) + 2 S_{\text{Ge-Se}}(Q) + S_{\text{Ge-Ge}}(Q). \qquad (4)$$

In Eq. (2) the summations are restricted to atoms of species α and β.

The second, third, and fourth peaks are a result of the short-range order of the model. This was determined by calculating $S(Q)$ from the local environment of each atom (all the atoms within a chosen spherical radius or correlation distance of an atom). The volume of the local environment is incrementally increased in order to observe the appearance of peaks in $S(Q)$. The third and fourth peaks appear as soon as the local environment includes nearest neighbors. These peaks, as well as peaks at higher Q, depend primarily on the nearest neighbors. The second peak depends on the next-nearest neighbors at approximately 3.8 Å. It is quite evident from the partial structure factors that the second peak is due to Se-Se correlations, thus it is the next-nearest-neighbor correlations between Se atoms which determine the shape of this peak; the $S_{\text{GeSe}}(Q)$ and $S_{\text{GeGe}}(Q)$ structure factors cancel each other.

The first sharp diffraction peak (FSDP) around 0.91 Å^{-1} is a result of correlations on a length scale of approximately 7.0 Å (this length is obtained from the FSDP's wave vector using $r = 2\pi/|\mathbf{Q}|$). From the $S_{\alpha\beta}(Q)$'s it is apparent that the FSDP has contributions from all of the partials, but $S_{\text{GeSe}}(Q)$ and $S_{\text{SeSe}}(Q)$ determine the peak position of the FSDP. The $S_{\text{GeGe}}(Q)$ contributes to the higher Q shoulder of the FSDP, broadening it. These results are in disagreement with x-ray scattering experiments on g-GeSe$_2$ (see Ref. 11) and neutron-diffraction experiments on liquid GeSe$_2$ (see Ref. 12). The analysis of Ref. 11 implies that the FSDP of g-GeSe$_2$ is due to Ge-Ge correlations only. The results of Ref. 12 imply that the FSDP in liquid GeSe$_2$ can be attributed to Ge-Ge correlations as well. Comparing these two results strongly suggests that Ge-Ge correlations are responsible for the FSDP of g-GeSe$_2$.

There is still a slight discrepancy between the experimentally observed strength of the second peak and that of our $S(Q)$. Overall our $S(Q)$ is in impressive agreement with the experimental results[10] in which $S(Q)$ is measured out to $Q = 35$ Å^{-1}. We will discuss the FSDP and its relationship to real-space structural properties further in Sec. III D.

B. Pair distribution functions

Partial pair-distribution functions (PDF's) $g_{\alpha\beta}(\mathrm{r})$ are defined in the same manner as those of Ref. 13. From $g_{\alpha\beta}(r)$ the the nearest-neighbor (average chemical bond length) and next-nearest-neighbor peaks are easily determined. The average coordination radii are determined from the position of first minimum. From Fig. 3 it is apparent that the average Ge-Se bond length of 2.37 Å is quite close to the crystal Ge-Se bond length of 2.355 Å (for α-GeSe$_2$) and that unlike the crystal there are Ge-Ge and Se-Se bonds.[10] The $g_{\text{Ge-Se}}(r)$ pair distribution becomes quite uniform after the nearest neighbor peak except for a peak around 5.7 Å. This second peak indicates that there is some kind of intermediate-range order within our model; the strength and width of this peak are due to Ge correlations with Se on neighboring tetrahedra.
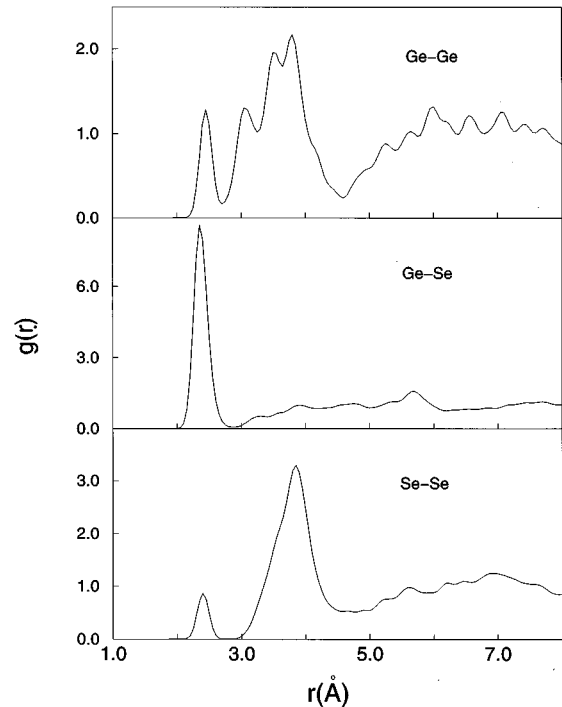

FIG. 3. Partial-pair distribution functions for 216 atom model.

The short-range order of the model is determined to a large extent by the 61% of the Ge atoms which form Ge(Se$_{1/2}$)$_4$ tetrahedra. In addition 25% form Ge$_2$Se$_6$ ethanes and 15% are threefold coordinated (only one of which is in an ethane configuration). There are two types of Se bonding defects, 10% are onefold coordinated and 20% are threefold coordinated. The threefold Ge atoms are correlated with onefold Se atoms at a distance of about 3.2 Å and show a much weaker correlation with other threefold Ge atoms at a distance of about 3.5 Å. This suggests that the threefold Ge atoms are mostly defective Ge(Se$_{1/2}$)$_4$ tetrahedra and not Ge$_2$Se$_6$ ethanes with long Ge-Ge bonds.

Mössbauer experiments[14] on bulk quenched prepared g-GeSe$_2$ samples using Sn as a Ge probe indicate that around 16% of the Ge atoms are not tetrahedrally coordinated by Se. It has been shown experimentally that the fraction of Ge-Ge bonds is much less in bulk quenched samples versus evaporation deposited thin films.[15,16] This higher percentage of Ge-Ge bonds we observe in our model suggests that the short-time scales of quenching for our model are closer to evaporation prepared films. It should be pointed out that the time scales of our molecular-dynamics approach is at most on the order of a few picoseconds, orders of magnitude faster then any laboratory method for creating g-GeSe$_2$ samples. This gives us a plausible explanation for the larger fraction of Ge-Ge bonds in our model.

We find that the fraction of Se atoms forming homopolar bonds is about twice what was seen in our earlier 62/63 atom models. About 20% of the Se atoms form dimers and another 5% form trimers. To our knowledge the exact fraction of Se-Se bonds has not been experimentally determined. Mössbauer experiments[17] using Te as a Se probe indicate that there are two distinct Se sites in bulk quenched g-GeSe$_2$; the two different sites being Ge-Se-Ge and Ge-Se-Se configurations. Raman experiments on evaporation deposited thin
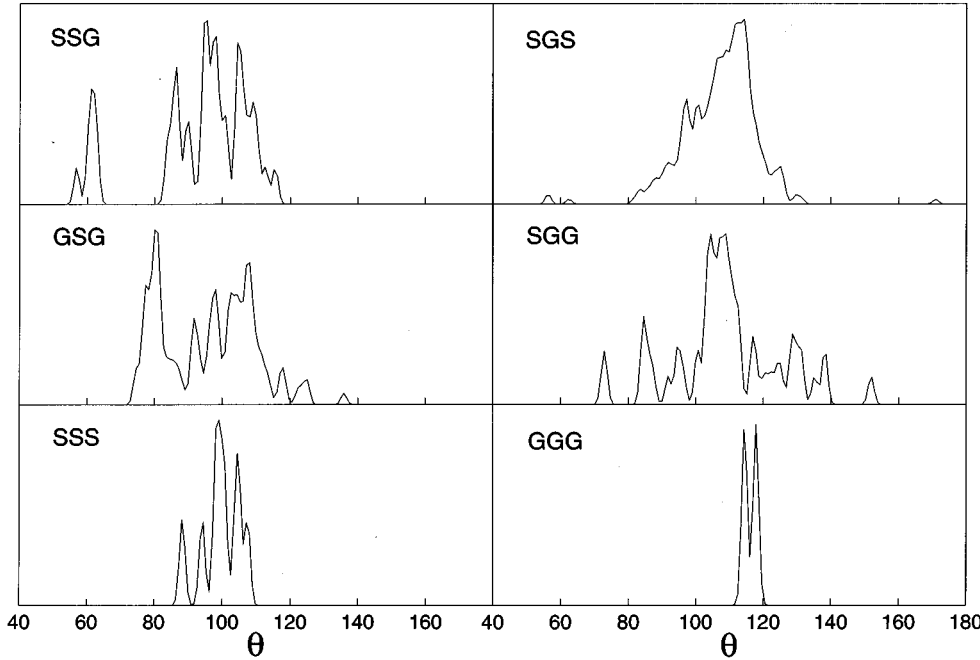
FIG. 4. Angle distributions for 216 atom model.

films and bulk quenched samples provide evidence for the existence of Se-Se bonds as well.[15] These experiments clearly show that vibrational modes near 33 meV attributed to Se-Se motion decrease as the thin films are annealed, becoming more like the bulk quenched samples. Similar results are observed for a peak associated with Ge-Ge motion located around 23 meV. It can be concluded from these results as well that homopolar bonds exist for both species and that their numbers are significantly less in annealed thin films and bulk quenched samples. The degree of chemical disorder in our model is much smaller then that of a random covalent network (RCN) (see Ref. 18). In a RCN Ge-Ge and Se-Se bonds each account for 25% of the total number of bonds. The Ge-Ge and Se-Se bonds in our model account, respectively, for only 3.5 and 7.4 % of the total number of bonds. This clearly shows that the chemistry of our model is not random and that the short-time scale of our model's creation did not prevent the correct chemistry from emerging.

The nearest-neighbor peak of $g_{Ge-Ge}(r)$ is located at approximately 2.46 Å. The next-nearest-neighbor peaks in $g_{Ge-Ge}(r)$ are due to correlations between Ge which share Se. This peak is rather wide due to the edge and corner configurations of both the $Ge(Se_{1/2})_4$ tetrahedra and Ge_2Se_6 ethanes. The three subpeaks can be attributed to the GSG angle distribution (which we will discuss in Sec. III C). The first peak at approximately 3.06 Å can be attributed to edge-sharing (fourfold rings) tetrahedra/ethanes. The GSG angle distribution (Fig. 4) has a single sharp peak associated with edge-sharing tetrahedra/ethanes and the average distance for edge-sharing Ge which form the angles of this peak is about 3.06 Å. The next two subpeaks at approximately 3.5 and 3.8 Å are due to corner sharing Ge configurations.

Experimental results indicate that approximately 40% of g-GeSe$_2$'s Ge atoms are in edge-sharing configurations.[10] These experimental results show a peak at 3.0 Å in the radial distribution function which is attributed to edge-sharing Ge atoms. As mentioned previously there is a peak in our $g_{Ge-Ge}(r)$ distribution around at 3.06 Å corresponding to the

edge-sharing tetrahedra/ethanes, thus the short-range order of our model is very similar to what is found experimentally. The 40% fraction of edge-sharing $Ge(Se_{1/2})_4$ tetrahedra (including threefold Ge) in our model agrees with experimental results for bulk quenched samples, but our model has an additional 7% edge-sharing Ge atoms in Ge_2Se_6 configurations as well.

The $g_{Se-Se}(r)$ nearest-neighbor peak is located at approximately 2.40 Å. The strength of this peak is about twice as large as what was observed in our earlier 62/63 atom models due to the larger number of homopolar bonds. Roughly 2/3 of the $g_{Se-Se}(r)$ distribution's second peak is due to correlations between Se atoms bonded to the same Ge atom. Correlations between Se atoms not bonded to the same Ge atom contribute the remaining 1/3 of this peak's strength. The second peak position at approximately 3.8 Å is identical to the Se-Se separation distance in crystalline α-GeSe$_2$ (Ref. 10).

C. Angle distribution functions

The various angle distributions were determined for all the possible nearest-neighbor configurations (see Fig. 4). Because the topology of the g-GeSe$_2$ is determined essentially by $Ge(Se_{1/2})_4$ tetrahedra and the manner in which they are linked together, the most significant angle distributions are those of the triads Ge-Se-Ge (GSG) and Se-Ge-Se (SGS). In order to better understand these statistics we determined angle distributions based on ring structures. The angles of a particular triad are assigned exclusively to the *smallest* ring structure they are part of. An angle is assigned to its lowest order ring structure on the assumption that these rings are the relevant ones to the short- and intermediate-range order. The ring structures in our model are determined by starting on an atom, moving to one of its neighbors, and then repeating this process for the neighbor until the original atom is located again after the desired number of iterations (making sure not to include any atom which is already part of the ring from a previous iteration). In Table I the number of n'th order rings

TABLE I. Ring statistics. The number of n-order rings, $n = 3$ through $n = 12$, and the number of these rings which contain 2–7 Se atoms.

Ring size	3	4	5	6	7	8	9	10	11	12
Number of rings	3	20	10	23	3	12	7	9	20	17
2 Se rings	3	20	2							
3 Se rings			8	20	1					
4 Se rings				3	2	10	4			
5 Se rings						2	2	8	14	2
6 Se rings							1	1	6	13
7 Se rings										2

from $n = 3$ to $n = 12$ are given as well as the number of these rings which have 2 (minimum number of Se) to 7 (maximum number of Se) Se atoms.

The GSG angle distribution has several peaks, the two most significant of these being at approximately 80° and 106°. The ring-order distributions reveal that GSG angles which are part of fourfold rings account almost entirely for the first peak at 80°. Interestingly a flat Ge-Se-Ge-Se four-fold ring with sides of length equal to our average Ge-Se bond length and GSG angles of 80° has Ge atoms which are 3.05 Å apart. We obtained a Ge-Ge separation of about 3.06 for edge sharing Ge atoms in our model and thus one can infer from this that the fourfold rings in our model are quite planar. Indeed visual inspection supports this conclusion.

Corner sharing Ge configurations account for the the rest of the angle distribution. The complexity of the GSG distribution can be understood in terms of ring structures (four, five, six, seven, or eightfold rings) as well as corner sharing Se atoms that only take part in higher (greater then eightfold) order rings. Apart from the peak at 80° arising from fourfold rings, the sixfold rings are the most significant ring structure for the GSG angles with contributions to all of the peaks except for the one around 135°. The peak around 118° is due entirely to sixfold rings. The fivefold rings contribute to the peaks around 92° and 106°. The five to eightfold rings and rings of higher order all contribute in some way to the peaks around 106°, the sixfold rings making the largest of these contributions. The sevenfold and eightfold rings contribute significantly to the peak at 125°. Angles which are only part of ring orders $n > 10$ also make significant contributions to the peak around 98°.

The SSG angle distribution is centered around a peak at approximately 95° and is quite similar to the SSS angle distribution. The SSG distribution is determined mainly by five-fold rings and angles which are only part of rings $n \geqslant 11$ with some small contributions from six and sevenfold rings. The peak around 60° is due to some rather odd threefold ring structures. The SSS angle distribution has most of its strength around 100° with very strong peaks at 99° and 104°. This is to be expected when one considers pure trigonal selenium. The trigonal form of selenium is composed of Se chains with SSS angles around 103° (Ref. 19). In our supercell there are two selenium chains (one with four Se and another with six Se) in which all the Se trimers take part except for two (which are not linked).

We do not present an extensive ring analysis of A-Ge-B angles since these angles are quite insensitive to the rings

structures which they are part of. The SGS angle distribution is peaked at 113°, close to the ideal tetrahedral angle of 109.5°, with smaller shoulder peaks at approximately 98° and 125°. The fourfold ring SGS angles are all located in the vicinity of the 98° peak and account for much of its strength. It is apparent from the width of the SGS distribution that there are significant bond angle distortions in the tetrahedra of our model.

The GGG and SGG angle distributions have their main peaks at 116° and 108°, respectively. Two of the Ge atoms have two Ge-Ge bonds and the angle distributions indicate that they are part of tetrahedral-like structures. The SGG angle distribution is quite similar to the SGS distribution as well. There appears to be a slight shift towards higher angles in the SGG distribution, indicated by the distribution strength around 125°.

D. Structural properties and the FSDP

The FSDP's of our previous 62/63 atom models were not as well defined as the FSDP of our 216 atom model. It would appear that a good description of g-GeSe$_2$'s intermediate-range order requires the larger supercell volume of the 216 atom model. Nevertheless it is still intriguing that the FSDP is reproduced so well by a 216 atom model with a cube edge of length 18.76 Å. The improvement of the FSDP parallels an improvement in the fraction of edge-sharing Ge atoms (fourfold rings) from 60% in our earlier models to 47% in our 216 atom model. The fraction of edge-sharing Ge atoms has been determined experimentally to be 40% (Ref. 10). A similar correlation between the FSDP and the fraction of edge-sharing Ge has been observed in other studies.[20,21] In these studies the fraction of edge-sharing tetrahedra was 5 and 32 % and there was significant improvement in the FSDP as the fraction of edge-sharing tetrahedra increased. There were no wrong bonds in these other studies, thus there would appear to be no significant correlation between the FSDP and chemical disorder. It is not obvious why the FSDP exhibits this dependence on the fraction of edge-sharing tetrahedra or why the fraction of edge-sharing Ge changes so dramatically with cell size in our studies, but it does provide one important insight into the origin of the FSDP in g-GeSe$_2$.

IV. DYNAMICAL PROPERTIES

The dynamical properties of our model are analyzed through the vibrational density of states (VDOS), species-projected VDOS, site projection of the normal modes, inverse participation ratio (IPR), the dynamical structure factor $S(Q,E)$ (DSF), and visual inspection of the normal modes. The VDOS and DSF can be determined through inelastic neutron scattering whereas the normal modes can only be inferred through a combination of experiment and theory. Because the VDOS and DSF can be determined experimentally they provide a straightforward test of our model's dynamical properties. Projection of the VDOS and the normal modes involves determining the contribution to the normal mode from a chosen set of atoms. The species-projected VDOS is determined by scaling the total VDOS at each energy with the contribution to the normal mode magnitude
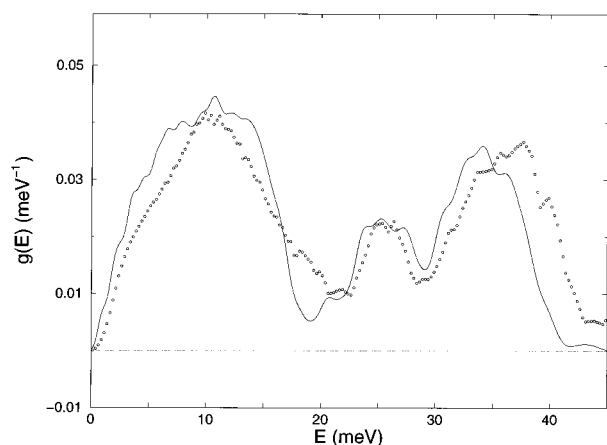
FIG. 5. Vibrational density of states: solid curve 216 atom model; open circles experimental data from Ref. 3.
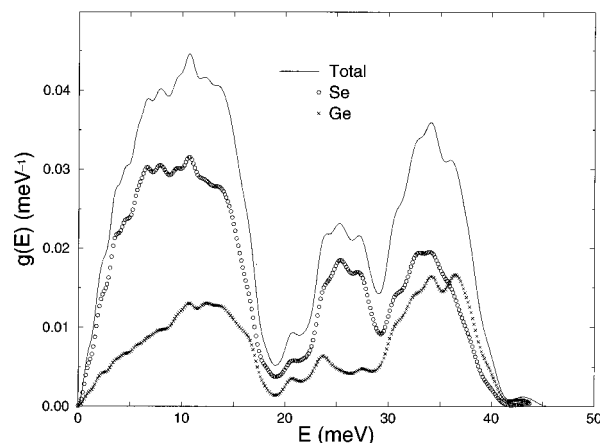

FIG. 6. Vibrational density of states and species projected vibrational density of states for Se and Ge for 216 atom model (open circles for Se and *x*'s for Ge).

from either the Ge or Se atoms. The localization of each normal mode is determined through the IPR. Computer visualization is used as well to obtain a qualitative understanding of the normal mode atomic motion.

The supercell normal mode eigenvalues and eigenvectors were obtained from the dynamical matrix. The dynamical matrix is determined by displacing each atom by 0.03 Å in three orthogonal directions and then performing *ab initio* force calculations for all the atoms for each such displacement. Each such calculation yields a column of the force constant matrix.[22] The vibrational eigenvectors and eigenvalues of the supercell are then easily obtained. The VDOS was determined from the vibrational eigenvalues by summing Gaussians centered at each eigenvalue; each Gaussian had a full width half maximum corresponding to the energy-dependent experimental resolution of Ref. 3.

A. Vibrational density of states and the normal modes

In our earlier 62/63 atom models we found good agreement between the vibrational density of states and the experimental inelastic neutron-scattering results.[3] Nevertheless discrepancies occurred between experimental neutron-scattering results and our 62/63 models in the 17–22 meV region. Beyond 34 meV the calculated VDOS of the 62/63 atom models and the experimental results disagreed as well. As seen from Fig. 5 there is good agreement between our 216 atom model and the experimental neutron-scattering results of Ref. 3. The 216 atom model VDOS improves upon our earlier work but still does not have the correct spectral weight in the 17–20 meV region and there is still a 2–4 meV redshift from experiment starting around 35 meV. We will discuss further the improvement of the 216 VDOS between 20 and 22 meV.

Experimentally determining the atomic motions of the normal modes can only be accomplished indirectly through Raman scattering, and thus our model offers a way of resolving controversies about the dynamics of particular peaks in the VDOS. We have focused our analysis on the regions of the VDOS which have been studied extensively through neutron and Raman scattering.[23,24] The main peaks observed in neutron-scattering experiments occur around 9, 11, 25.7, 33, and 36 meV with weaker features around 18.5 and 39 meV

(see Ref. 3). The 25.7 meV peak is split such that it has two peaks around 25 and 27 meV referred to as the A_1 and A_{1c}.

Based on Raman measurements the 25 meV peak has been associated with the A_1 tetrahedral breathinglike motion (see Ref. 25). An interpretation of the 27 meV peak has proved more difficult. It has been hypothesized that the A_{1c} motion of Se atoms connecting edge-sharing tetrahedra are responsible for the 27 meV peak.[25] In our model the normal modes of the A_1 band (24.37–26.43 meV) and the A_{1c} band (26.43–29 meV) appear to be dominated by tetrahedral breathinglike motions. There is a qualitative difference between A_1 and A_{1c} atomic motion of edge-sharing tetrahedra. In the A_{1c} the atomic motion of Se which link the edge-sharing tetrahedra has more of a bond-bending quality as opposed to the bond stretching seen in the A_1. This was determined through direct visual inspection of the normal mode atomic motion using the program XMOL (Ref. 26). Animating the normal modes gives us a good qualitative understanding of their dynamics. Additional insight is provided by the species-projected density of states (Fig. 6). The species-projected VDOS for the Se and Ge atoms clearly show that the Se atoms are responsible for most of the motion in the 24–28 meV range. The ratio of the Ge and Se species-projected VDOS reaches its minimum value at 25.6 meV which is consistent with the tetrahedral breathinglike motion observed using XMOL.

The peak around 20 meV has been interpreted as an ethane Ge-Ge stretch mode based on Raman measurements.[15] About 60% of the modes in the 18–23 meV region are highly localized on threefold Ge and/or their nearest neighbors; this type of localization was observed in our previous work as well.[3] In 22% of the 18–23 meV modes there is significant localization on ethanes. Modes involving ethane motion represent a new type of normal mode not seen in our earlier models due to the absence of Ge-Ge bonds. In 19% of the modes in the 18–23 meV region (see Fig. 7) Ge-Ge motion accounts for approximately 15% of the total mode magnitude; these modes do not have a large degree of localization on any particular ethane, but rather an increased weight on a number of ethanes. In a perfectly extended mode
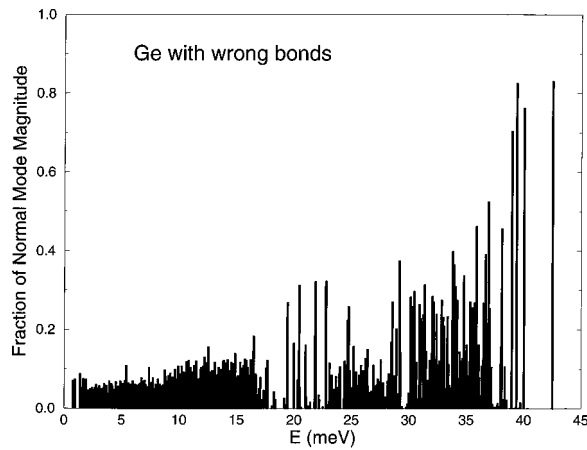
FIG. 7. Fraction of normal mode magnitude as a function of mode energy for Ge atoms with wrong bonds.

FIG. 9. Vibrational density of states and scaled inverse participation ratio histogram for the 216 atom model.

the contribution of Ge-Ge motion to the total mode magnitude would only be about 8%. This suggests it is the ethanes which account for the significant improvement between our 216's VDOS and experiment in the 20-22 meV region and why our earlier models did not compare very well to the experimental data for this region. This appears to confirm the experimental conjecture that Ge-Ge stretch modes contribute significantly to the modes of the 20 meV region.

The general kind of tetrahedral motion which was observed throughout the 29–41 meV region resembles the F_2 mode of an isolated tetrahedron.[27] This type of motion involves the Ge atom moving towards two of its Se neighbors (which are moving towards it as well), while its two other Se neighbors move away from it. As seen from Fig. 6 the Se and Ge species-projected VDOS are similar in this energy range and therefore consistent with F_2-type motion. In addition there are a number of modes which are highly localized on Se atoms with homopolar bonds; Se atoms with homopolar bonds contribute significantly to the mode amplitudes in this region of the VDOS as seen from Fig. 8. Ge atoms with homopolar bonds contribute to the modes of this region as well and in particular there is a band of highly localized
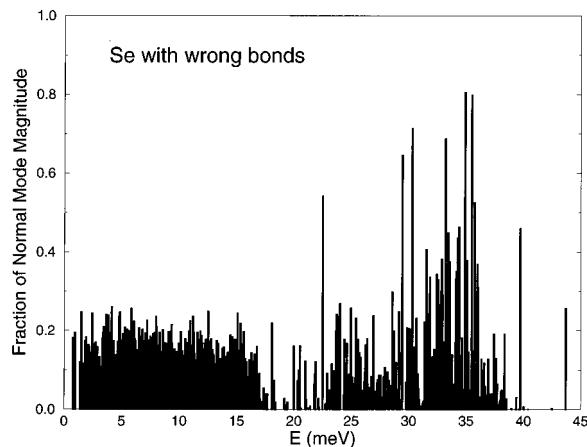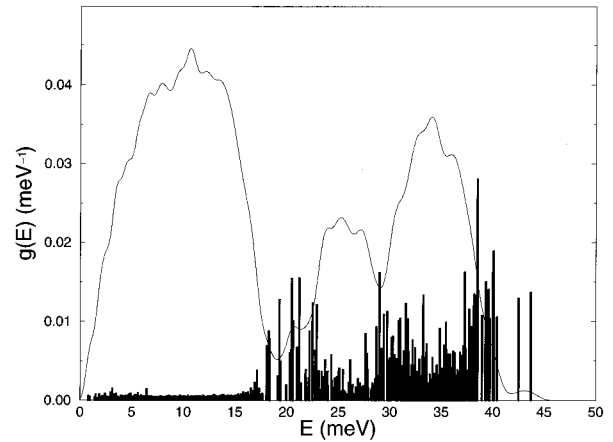
modes around 39 meV involving ethanes (see Fig. 7). These results are consistent with those of previous Raman studies.[15,23,24]

The IPR has a value of 1 for a completely localized state and a value of $1/3N$ (1.54×10^{-3} for $N = 216$) for a completely extended state. A trend of intense localization in regions of decreasing spectral density (band tails) is apparent from Fig. 9 in which the IPR is *scaled* and plotted against the VDOS. The IPR (Fig. 10) is less then 10^{-2} for almost all the modes below mode 333 (15.5 meV) and greater then 10^{-2} for almost all the modes above this energy. The same type of dramatic transition was seen in the IPR of our previous work as well.[3] A plausible explanation for this transition can be found in the types of motion which occur above and below 15.5 meV. There are two general types of VDOS motion: (1) extended modes (< 15.5 meV) involving the motion of entire tetrahedral units and (2) more localized modes (> 15.5 meV) involving internal tetrahedral motions (e.g., tetrahedral breathing, F_2-type motion). One might expect a higher degree of localization for modes which involve local structural properties of the supercell topology as opposed to modes which involve the motion of larger regions of the supercell.
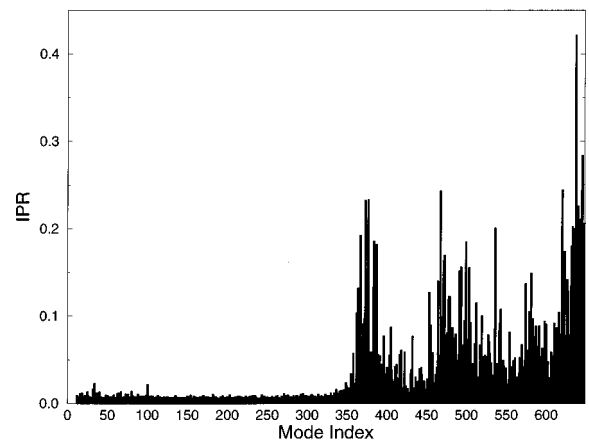

FIG. 8. Fraction of normal mode magnitude as a function of mode energy for Se atoms with wrong bonds.

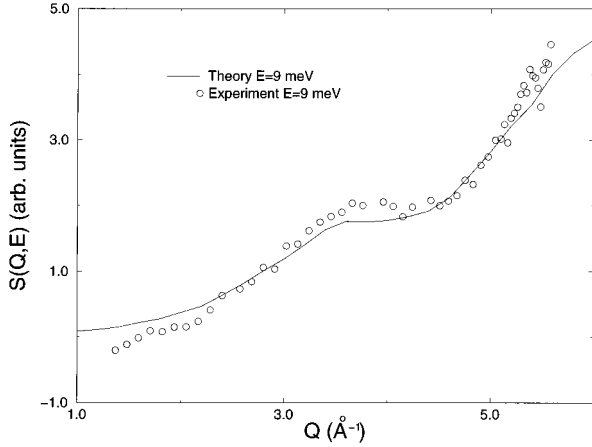FIG. 10. Vibrational inverse participation ratio of 216 atom model.

FIG. 11. $S(Q,E)$ for 9 meV. Open circles indicate experimental neutron-scattering data from Ref. 3.

B. Dynamical structure factor

A direct comparison between theory and experiment can be obtained through the dynamical structure factor $S(Q,E)$. The theoretical dynamical structure factors were computed from Eq. (8) of Ref. 23 with the same neutron-scattering lengths used for $S(Q)$. We find good agreement between our $S(Q,E)$ and the experimental neutron-scattering data of Ref. 3 for 9 meV (Fig. 11), the A_1 and A_{1c} regions (Fig. 12), and higher energies of 32.71, 35.88, and 39.4 meV (Fig. 13). These dynamical structure factors were calculated with an energy resolution of 1.6 meV corresponding to the experimental resolution of Ref. 3 at 25 meV.

In Ref. 23 $S(Q,E)$ generated from the normal modes of a single Ge(Se$_{1/2})_4$ tetrahedra are very similar to experimental data at 39.9 meV and qualitatively similar to results at 25.91 meV. They identify the 25.91 meV motion as the A_1 tetrahedral breathing mode and the 39.9 meV motion as the F_2 tetrahedral mode. This gives support to our visual observations of tetrahedral breathinglike motion around 25 meV and F_2-like motion in the 29–41 meV region. As pointed out in Ref. 23 the experimental $S(Q,E)$ around 33, 36, and 39 meV
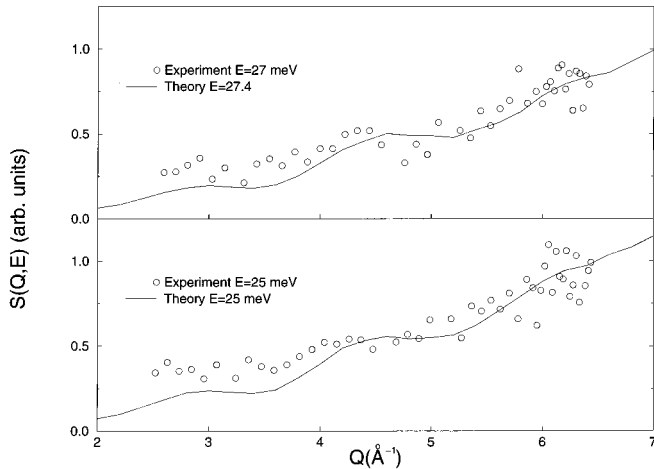

FIG. 12. $S(Q,E)$ for A_1 (25 meV) and A_{1c} (27.4 meV) regions. Open circles indicate experimental neutron-scattering data from Ref. 3.
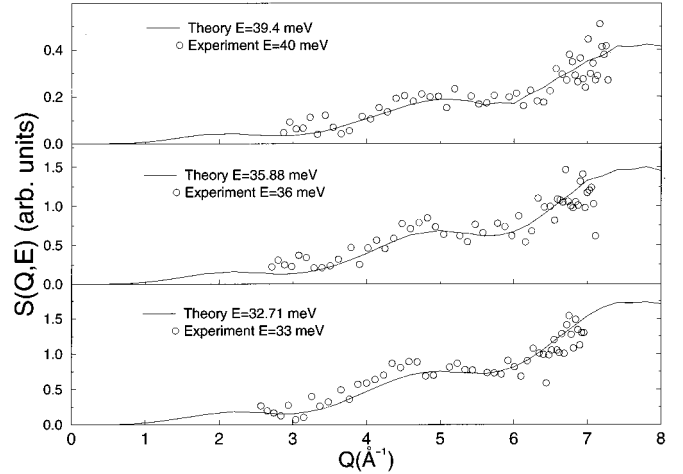

FIG. 13. $S(Q,E)$ for 32.71, 35.88, and 39.4 meV. Open circles indicate experimental data from Ref. 3.

are all quite similar, suggesting F_2-like motion at all of these energies. The features of our theoretical $S(Q,E)$ in the 29–41 meV range are quite invariant as seen from Fig. 13 in agreement with the experimental results of Refs. 3 and 23 and our normal mode visualization. It should be pointed out that while $S(Q,E)$ indicates qualitative trends in the dynamics it is *remarkably insensitive* to the fine structure which exists in the VDOS, a fact which is certainly evident from the $S(Q,E)$ plots in Figs. 12 and 13.

V. ELECTRONIC STRUCTURE

Our electronic density of states (EDOS) in Fig. 14 agrees quite well with experimental results obtained from x-ray photoemission spectroscopy (XPS) (Ref. 28) and ultraviolet photoemission spectroscopy (UPS) (Ref. 29) measurements as well as with those obtained in earlier theoretical studies.[28,30–32] The models of g-GeSe$_2$ presented in Refs. 30,31 were large scale models based on high-temperature forms of crystalline GeSe$_2$ (48 atom layered structure). In both these models there is a substantial splitting between the first two peaks of the valence band (the A_1 and A_2 peaks,
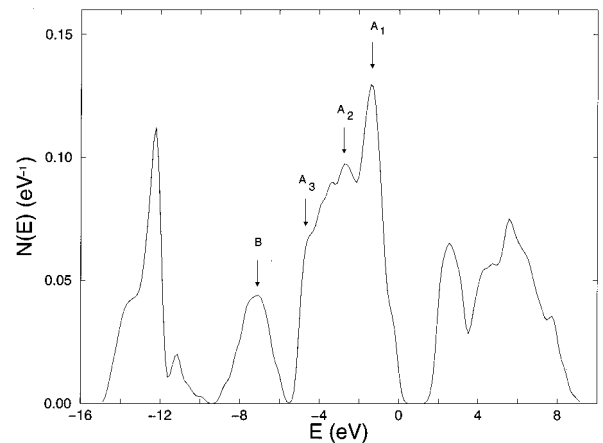

FIG. 14. Theoretical electronic density of states. Valence-band edge is at zero (see text for details).

TABLE II. The positions of the A_1, A_2, A_3, and B peaks in the electronic density of states of our model compared to the experimental results of Ref. 29.

(eV)	A_1	A_2	A_3	B
Theory	-1.4	-2.7	-4.6	-7.0
Experiment	-1.38	-3.0	-4.6	-7.8

respectively). The A_1 and A_2 peaks of our model do not have this high degree of separation and are in better agreement with the experimental data. The assignment of the A_3 peak was made by comparing XPS and UPS data. The XPS result of Ref. 28 is quite similar to our EDOS, indicating that the A_3 peak should be assigned to the shoulder of the valence band peak and not to the small peak just to the left of the A_2. The two other main peaks around -12.3 and -7.3 eV (the B peak) are in good agreement with the XPS results as well. The theoretical peak positions are listed in Table II (indicated by arrows in Fig. 14) with those obtained from UPS measurements[29] (where our electronic eigenvalues have been shifted in order to place the valence-band-edge eigenvalue at zero). The EDOS was obtained by summing suitably broadened Gaussians centered at each eigenvalue.

The Γ-point optical band gap of our model is 1.72 eV which is approximately 0.2–0.5 eV less then the experimentally determined optical gap of evaporation deposited and annealed thin films, respectively.[1,16,33] It has been shown experimentally that the optical gaps of a g-GeSe$_2$ thin films increase when they are annealed.[1,16] Since our model is structurally similar to an evaporation deposited thin film one would expect the band gap to be smaller then that of a bulk sample. It is quite remarkable that there are *no states in the fundamental band gap* considering the number of topological defects in our model. Very small concentrations of midgap states (10^{15}–10^{17}/cm^3), detected through electron-spin resonance and dc conductivity measurements, have been attributed to Ge and Se coordination defects.[1,4] For the ideal case of an impurity free sample one would have to question this interpretation of the observed gap states.

We determine the localization of our electronic eigenvalues through an inverse participation ratio

$$q_2(E_i) = \sum_{n=1}^{N} q(n, E_i)^2, \tag{5}$$

such that $q_2(E)$ equals 1 for completely localized states and $1/N$ (N being the total number of atoms) for completely delocalized states (Fig. 15). The charge localization at atomic site n for eigenvalue E_i is determined from $q(n, E_i)$. For details we refer the reader to Ref. 34. The number of eigenvalues in the peaks centered around -12.3 and -7.3 eV is equal to the number of Se and Ge atoms, respectively. The Se and Ge $q_2(E)$'s (Fig. 15) reveal that the localization of the -12.3 eV peak is on Se atoms and for the -7.3 eV peak it is on Ge atoms. The eigenstates of the main peak at -12.3 eV are not highly localized and are associated with Se atoms that do not have homopolar bonds. The eigenstates of the small subpeak around -11 eV are all highly localized and occur predominantly on Se atoms with homopolar bonds and/or overcoordination. There is a small
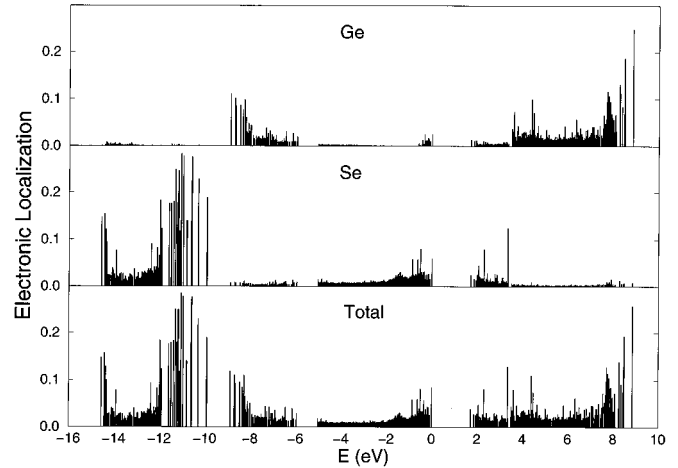

FIG. 15. Localization of electronic eigenstates. The total localization, localization on Se, and localization on Ge are shown. Valence-band edge is at zero.

band of highly localized states on singly coordinated Se atoms centered around -12 eV. The eigenvalues from -10.8 to -9.8 eV, at the edge of the gap separating the Se and Ge localized states, are localized on Se trimers. The Se trimers also account for a thin band of highly localized states around -14.5 eV, the lowest energy electronic states. The highly localized Ge states around -8.5 eV occur almost entirely on Ge atoms with homopolar bonds. There are significantly more states bordering both sides of the gap between Se and Ge states in the 216 atom model than in our 62/63 atom models. This can be attributed to the larger fraction of Se homopolar bonds and the appearance of Ge homopolar bonds in the 216 atom model.

Eigenstates of the valence-band peak between -5.0 and -1.6 eV are quite extended, but as one approaches the valence-band edge the eigenstates become increasingly localized as seen from Fig. 15. The Ge $q_2(E)$ peak near the valence band edge is due almost entirely to undercoordinated Ge atoms, while the Se localization is more complex and does not appear to involve just one type of defect, although there is significant localization on atoms that are singly coordinated and those that have homopolar bonds. As seen from Fig. 15 the conduction band states are more localized on Se, with highly localized states on Se atoms that are overcoordinated or those that have homopolar bonds. Beyond the first main peak of the conduction band the eigenstates become localized essentially on Ge atoms.

These results are similar in character to a model put forth by Lannoo and Bensoussan in Refs. 28,32, which predicted that the low-energy peaks should consist of Se and Ge $4s$-orbital states with a splitting of 6 eV between these peaks. The experimental UPS data for crystalline Ge and Se in Ref. 28 support our model as well. Crystalline Ge has a peak corresponding to our -7.3 eV peak, but lacks a peak corresponding to our -12.3 eV peak, while the situation is exactly the opposite in crystalline Se. Their model predicts Ge-Se bonding states in the valence-band with Se lone-pair electron states at the valence-band edge. They also predict that the conduction band will have Se and Ge-Se antibonding states with the Se states at the conduction band edge.

VI. CONCLUSION

We find that our 216 atom model improves upon the structural and vibrational results of our earlier study[3] when compared to experiment. The FSDP and the fraction of edge-sharing tetrahedra clearly indicate that the topology of our 216 model is closer to experiment. In addition the fraction of wrong bonds for both species increased in the 216 atom model. We conclude from this that our model's chemical disorder is very similar to that of an evaporation deposited thin film as opposed to a bulk quenched sample. Evidently the larger 216 supercell allows the correct chemistry and topology to emerge.

The dynamics of the current model are closer to experiment as evidenced by the improvements in the VDOS. The spectral weighting of the 20–40 meV region is noticeably better then our earlier 62/63 atom models. Yet, there is still a redshift between the VDOS and the experimental neutron scattering data at higher energies. Our analysis of the normal modes reveals a trend of localization in the band tails of the VDOS as well as a significant change in the degree of localization for modes above approximately 15.5 meV. The qualitative types of atomic motion which exist in the A_1, A_{1c}, and 30–40 meV regions have been determined through visual inspection of the normal modes. We find that the results obtained from visualization are consistent with inelastic neutron-scattering and Raman measurements. Normal mode analysis also shows that chemical disorder has a significant effect on the dynamics g-GeSe$_2$.

The electronic structure of our model is in good agreement with experiment and more importantly there are no gap states observed in our EDOS despite the large number of topological defects which exist. The lack of gap states in our model suggests that such states are highly improbable in pure g-GeSe$_2$. In conclusion we find that our larger 216 atom model improved upon the results of our earlier study in its description of g-GeSe$_2$'s structural, vibrational, and electronic properties, indicating that deficiencies associated with finite-size effects have for the most part been overcome.

[1] K.M. Kandil *et al.*, Phys. Rev. B **51**, 17 565 (1995).

[2] Johannes Sarnthein, Alfredo Pasquarello, and Roberto Car, Phys. Rev. Lett. **74**, 4682 (1995).

[3] R. L. Cappelletti, Mark Cobb, D. A. Drabold, and W. A. Kamitakahara, Phys. Rev. B **52**, 9133 (1995).

[4] R. A. Street and D. K. Biegelsen, J. Non-Cryst. Solids **32**, 339 (1979).

[5] Otto F. Sankey and D. J. Niklewski, Phys. Rev. B **40**, 3979 (1989); Otto F. Sankey, D. A. Drabold, and G. B. Adams, Bull. Am. Phys. Soc. **36**, 924 (1991).

[6] G. B. Bachelet, D. R. Hamann, and M. Schlüter, Phys. Rev. B **26**, 4199 (1982).

[7] J. Harris, Phys. Rev. B **31**, 1770 (1985).

[8] Peter Fulde, *Electron Correlations in Molecules and Solids*, 2nd ed. (Springer-Verlag, New York, 1993), p. 44.

[9] Alexander A. Demkov *et al.*, Phys. Rev. B **52**, 1618 (1995).

[10] S. Susman *et al.*, J. Non-Cryst. Solids **125**, 168 (1990).

[11] A. Fischer-Colbrie and P. H. Fuoss, J. Non-Cryst. Solids **126**, 1 (1990).

[12] Ian T. Penfold and Philip S. Salmon, Phys. Rev. Lett. **67**, 97 (1991).

[13] N. E. Cusak, *The Physics of Structurally Disordered Matter* (Adam Hilger, Bristol, 1987), pp. 35 and 36.

[14] M. Stevens, P. Boolchand, and J.G. Hernandez, Phys. Rev. B **31**, 981 (1985).

[15] R. J. Nemanich *et al.*, Phys. Rev. B **18**, 6900 (1978).

[16] Didarul Islam and R. L. Cappelletti, Phys. Rev. B **44**, 2516 (1991).

[17] W. J. Bresser, P. Boolchand, P. Suranyi, and J. P. de Neufville, Phys. Rev. Lett. **46**, 1689 (1981).

[18] S. R. Elliot, *Physics of Amorphous Materials*, 2nd ed. (Longman Scientific and Technical, New York, 1990), pp. 134 and 135.

[19] R. Martin, G. Lucovsky, and K. Helliwell, Phys. Rev. B **13**, 1383 (1976).

[20] P. Vashishta, Rajiv K. Kalia, and I. Ebbsjö, Phys. Rev. B **39**, 6034 (1989).

[21] P. Vashishta *et al.*, Phys. Rev. Lett. **62**, 1651 (1989).

[22] O. F. Sankey (unpublished).

[23] U. Walter, D. L. Price, S. Susman, and K. J. Volin, Phys. Rev. B **37**, 4232 (1988).

[24] P. M. Bridenbaugh, G. P. Espinosa, J. C. Phillips, and J. P. Remeika, Phys. Rev. B **20**, 4140 (1979).

[25] S. Sugai, Phys. Rev. B **35**, 1345 (1987).

[26] XMOL, version 1.3.1, 1993, Minnesota Supercomputer Center, Inc., Minneapolis, MN 55415.

[27] P. N. Sen and M. F. Thorpe, Phys. Rev. B **15**, 4030 (1977).

[28] E. Bergignat *et al.*, Phys. Rev. B **37**, 4506 (1988).

[29] S. Hino, T. Takaharshi, and Y. Harada, Solid State Communi. **35**, 379 (1980).

[30] Steven G. Louie, Phys. Rev. B **26**, 5993 (1982).

[31] Willian Pollard, J. Non-Cryst. Solids **144**, 70 (1992).

[32] M. Lannoo and M. Bensoussan, Phys. Rev. B **16**, 3546 (1977).

[33] D. E. Aspnes *et al.*, Phys. Rev. B **23**, 816 (1981).

[34] Attila Szabo and Neil S. Ostlund, *Modern Quantum Chemistry* (McGraw-Hill, New York, 1989), p. 151.